REGULAR ARTICLE

Synthesis, Structure Investigation, Spectral Characteristics and Biological Activities of 4-benzyl-3-(2-hydroxyphenyl)-1H-1,2,4-triazole-5(4H)-thione

Metin Koparir ^{1*}, Cahit Orek ¹, Naci Ömer Alayunt ¹, Akif Evren Parlak ¹, Pelin

Koparir ², Kamiran Sarac ³, Sevgi Durna Dastan⁴, Nevin Cankaya⁵

This **Abstract:** work presents characterization 4-benzyl-3-(2the of hydroxyphenyl)-1*H*-1,2,4-triazole-5(4*H*)-thione (III) by quantum calculations and spectral techniques. The molecular geometry, vibrational frequencies and gauge including atomic orbital (GIAO) ¹H and ¹³C NMR chemical shift values of III in the ground state have been calculated using the density functional method (B3LYP) with the 6-31G(d,p) basis set. To determine conformational flexibility, the molecular energy profile of the title compound was obtained by using B3LYP/6-31G(d,p) method with respect to the selected torsion angle, which was varied from -180° to +180° in steps of 10°. The calculated results show that the optimized geometry can well reproduce the crystal structure, and the theoretical vibrational frequencies and chemical shift values show good agreement with experimental values. In addition, DFT calculations of molecular electrostatic potentials and frontier molecular orbitals of III were carried out at the

¹ Firat University, Faculty of Science, Department of Chemistry, 23119, Elazig, Turkey

² Department of Chemistry, Forensic Medicine Institute, 44000, Malatya, Turkey

³ Inönü University, Faculty of Science, Department of Chemistry, 44100, Malatya, Turkey

⁴ Cumhuriyet University, Faculty of Science, Department of Biology, 58140, Sivas, Turkey

⁵ Usak University, Faculty of Science and Arts, Department of Chemistry, 64100, Usak, Turkey Received 6 February 2013; Accepted (in revised version) 13 May 2013

^{*} Corresponding author. *E-mail address:* <u>mkoparir@hotmail.com</u> (M.Koparir). <u>http://www.global-sci.org/cicc</u>

B3LYP/6–31G(d,p) level of theory. The title compound was screened for antibacterial, antifungal and antioxidant activities.

AMS subject classifications: 81-08, 97M60

Key word: 4-Benzyl-3-(2-hydroxyphenyl)-1*H*-1,2,4-triazole-5(4*H*)-thione, Density-Functional Theory, Crystal-Structure, Ab-initio, Antimicrobial activity

1 Introduction

Triazole and its derivatives represent an important class of heterocycles. They are of biological important and are used in the synthesis of drugs [1,2]. A number of 1,3,4-thiadizoles showed antibacterial properties similar to those of well-known sulphonamide drugs [3]. Thus the thiadiazole nucleus, which incorporates an N-C-S linkage, exhibits a large number of biological activities [4]. Derivatives of 1,2,4-triazole have been reported to exhibit diverse biological activities [5–11]. Triazole derivatives are also used in the synthesis of antibiotics, fungicides, herbicides, plant growth hormone insulators [12] and potentially good corrosion inhibitions [13,14]. In addition there are some studies on electronic structures and thiol-thione tautomeric equilibrium of heterocyclic thione derivatives [15–16]. 1,2,4-Triazoles are very useful ligands in coordination chemistry. The utilization of the 1,2,4-Triazole moiety as a part of ligand system in metal complexes has gained considerable attention in recent years [17–19]. The application of triazole ligand lies in medical research-complex with Pt(II) [20] exhibit antitumor activity (human cancer) similar to *Cisplatin*.

Density functional theory (DFT) has been one of the widely used theories in theoretical modeling during recent years. By means of the development of better exchange-correlation functionals, it has become possible to calculate many molecular properties which have accuracies that can be comparable to traditionally correlated *ab initio* methods, all these could be done with more favorable computational costs [21]. It has been figured out during the literature survey that in reproducing the experimental values in geometry, dipole moment, vibrational frequency etc. DFT has a precise accuracy [22-26].

The aim of this study is to investigate the energetic and structural properties of the 4-benzyl-3-(2-hydroxyphenyl)-1*H*-1,2,4-triazole-5(4*H*)-thione (**Figure 1**), using density functional theory calculations. In this study, the optimized geometry, vibrational spectra and assignments, molecular electrostatic potential (MEP) and the statistical energetic parameters of **III** have been studied. These calculations are valuable for providing insight into molecular properties of 1,2,4-triazole compounds. Besides the characterization of the title compound, the biological activities of the **III**, such as antibacterial, antifungal and antioxidant activities were investigated.

Figure 1: Chemical diagram of 4-benzyl-3-(2-hydroxyphenyl)-1H-1,2,4-triazole-5(4H)-thione.

2 Experimental

2.1 Synthesis

For the synthesis of (**II**), a mixture of (**I**) (0.01 mol) and benzyl isothiocyanate (0.01 mol) in absolute ethanol (100 ml) was refluxed for 8 h. The solid material obtained on cooling was filtered off, washed with diethyl ether, dried and crystallized from ethanol-dioxane (yield 84%; m.p. 487 K). IR (v, cm⁻¹): 3425, 3300 (N–H, O–H), 1672 (C=O), 1262 (C=S). For the synthesis of (**III**), a stirred mixture of (**II**) (0.01 mol) and sodium hydroxide (0.01 mol, as a 2 N solution) was refluxed for 4h. After cooling, the solution was acidified with hydrochloric acid and the precipitate was filtered off. The precipitate was then crystallized from a methanol–dioxane mixture (yield 95%; m.p. 471–473 K). IR (v, cm⁻¹): 3298 (O–H), 3216 (N–H), 1628 (C=N). ¹H NMR (400MHz, DMSO-*d*₆, 24°C): 5.16 (s, 2H, N-CH₂), 6.79–7.34 (m, 9H, Ar-H), 10.40 (s, 1H, OH), 13.94 (s, 1H, NH). Elemental analysis: C, 63.55; H, 4.60; N, 14.85.

2.2 Physical measurements

Melting points were determined on a Thomas Hoover melting point apparatus and uncorrected, but checked by differential scanning calorimeter (DSC). KBr pellets on a Perkin–Elmer Spectrum one FT–IR spectrophotometer was used in order to record FT-IR spectra of III in 4000–400 cm⁻¹ region. Electronic spectral studies were conducted on a Shimadzu model UV-1700 spectrophotometer in the wavelength 1100–200 nm. The ¹H and ¹³C spectra were taken on Bruker AC-400 NMR spectrometer operating at 400 MHz for ¹H-, 100 MHz for ¹³C-NMR. Elemental analyses were done on a LECO-CHNS-938. Compound was dissolved in DMSO-*d*⁶ and chemical shifts were referenced to TMS (¹H and ¹³C NMR). Starting chemicals were provided by Merck or Aldrich. The synthesis reaction of III is shown in Figure 2.

$$\begin{array}{c} O \\ O \\ C \\ OH \end{array} + \begin{array}{c} O \\ C \\ OH \end{array} + \begin{array}{c} O \\ C \\ OH \end{array} + \begin{array}{c} O \\ C \\ OH \end{array} - \begin{array}{c} O \\ OH \\ OH$$

Figure 2: The reaction for the synthesis of title compound.

2.3 Antibacterial activity

The synthesized compound III was screened for their antibacterial activity against Escherichia coli (ATTC-25922), Staphylococcus aureus (ATTC-25923), Pseudomonas aeruginosa (ATCC-27853) and Klebsiella pneumoniae (recultured) bacterial strains by serial plate dilution method [27,28]. Serial dilutions of the drug in Muller-Hinton broth were taken in tubes and their pH was adjusted to 5.0 using phosphate buffer. Standardized suspension of the test bacterium was inoculated and incubated for 16-18 h at 37 °C. The minimum inhibitory concentration (MIC) was noted by observing the lowest concentration of the drug at which there was no visible growth. A number of antimicrobial discs are placed on the agar for the sole purpose of producing zones of inhibition in the bacterial lawn. Agar media were poured into each Petri dish. Excess of suspension was decanted and placing in incubator at 37 °C for 1 h dried the plates. Using an agar punch, wells were made on these seeded agar plates and minimum inhibitory concentrations of the test compounds in DMSO were added into each labeled well. A control was also prepared for the plates in the same way using DMSO as solvent. The Petri dishes were prepared in triplicate and maintained at 37 °C for 3-4 days. Antibacterial activity was determined by measuring the diameter of inhibition zone. Activity of each compound was compared with Ciprofloxacin as standard [29,30]. Zone of inhibition was determined for title compound the results are summarized in Table 1.

6.25 (16-20)

1.56 (22-30)

Commound	MIC	Cin μg/mL and zoι	ne of inhibition (m	nm)
Compound	E.coli	K. pneumoniae	P. aeruginosa	S. aureus
Title Compound	12.50 (11–15)	12.50 (11–15)	6.25 (16-20)	6.25 (16-20)
Ciprofloxacin	6 25 (16-20)	6 25 (16-20)	6 25 (16-20)	1 56 (22-30)

6.25 (16-20)

Table 1 Minimum inhibitory concentration (MIC, µg/mL) data of the title compound against a number of bacteria.

Note: the MIC values were evaluated at concentration range, 1.56–25 µg/mL.

6.25 (16-20)

2.4 Antifungal activity

Newly prepared compound was screened for their antifungal activity against Aspergillus flavus [NCIM No.524], Aspergillus fumigatus [NCIM No. 902], Penicillium marneffei [recultured] and Trichophyton mentagrophytes [recultured] in DMSO by serial plate dilution method [31]. Agar media were prepared by dissolving peptone (1 g), D-glucose (4 g) and agar (2 g) in distilled water (100 mL) and adjusting the pH to 5.7. Normal saline was used to make a suspension of spore of fungal strains for lawning. A loopful of particular fungal strain was transferred to 3 mL saline to get a suspension of corresponding species. Agar media of 20 mL were poured into each Petri dish. Excess of suspension was decanted and plates were dried by placing in an incubator at 37 °C for 1 h. Using an agar punch each labeled well were made on these seeded agar plates and MIC of the test compounds in DMSO were added into each labeled well. A control was also prepared for the plates in the same way using solvent DMSO. The Petri dish were prepared in triplicate and maintained at 37 °C for 3–4 days. Antifungal activity was determined by measuring the diameter of the inhibition zone. Activity of each compound was compared with Ciclopiroxolamine as standard. Zones of inhibition were determined for title compound the results are summarized Table 2.

Table 2 Antifungal activity of title compound.

Commound	MIC in μg/mL and zone of inhibition (mm)			
Compound	Compound P. marneffei T. mentagrophytes		A. flavus	A. fumigatus
Title Compound	12.50 (11-15)	6.25 (16-20)	12.50 (11-15)	12.50 (11-15)
Ciclopiroxolamine	6.25 (16-20)	3.125 (27-33)	3.125 (25-30)	6.25 (16-20)

Note: the MIC values were evaluated at concentration range, 1.56–25 µg/mL.

2.5 DPPH free radical scavenging activity

Free radical scavenging activity of the title compound was determined by measuring the change in the absorbance of DPPH• (1,1-diphenyl-2-picrylhydrazylradical) at 517 nm spectrophotometrically. Stock solutions of 500 µM of tested sample and DPPH• were prepared in DMSO. 400 µL of DPPH• solution was added to sample solution at different concentrations (500, 1000, 1500, 2000 and 2500 µL) and appropriately diluted with DMSO to total volume of 4.0 mL. A 400 µL from DPPH• stock solution was also diluted to 4.0 mL using DMSO as solvent to make the control. The reaction mixtures were thoroughly mixed by shaking the test tubes vigorously and incubated at 25 °C for 60 min in a water bath in the dark. Absorbance at 517 nm was measured and the solvent was corrected throughout. Ascorbic acid was used as a standard (using the reference antioxidant) for this test. The DPPH (1,1-diphenyl-2-picrylhydrazyl) radical scavenging method was chosen to determine the antioxidant potential of the target compounds in comparison with the commercially available antioxidant Ascorbic acid at the same concentrations. The scavenging effect was calculated using the following equation [32]:

Scavenging activity (%) =
$$\frac{A_0 - A_s}{A_0}$$
 x 100

where A_s is the absorbance of the DPPH $^{\bullet}$ in the presence of the tested compound and A_0 is the absorbance of the DPPH $^{\bullet}$ in the absence of the tested compound (control). The data for antioxidation presented as means \pm SD of three determinations.

2.6 Computational methods

The molecular geometry was taken directly from the X-ray diffraction result unrestrainedly. In the following step, the Gaussian 09W software package [33] was used to make the DFT calculations with a hybrid functional B3LYP (Becke's Three parameter hybrid functional by means of the LYP correlation functional) with the 6-31G(d,p) basis set using the Berny method [34-35]. At the same level of the theory, the harmonic vibrational frequencies for the optimized structure were assessed and the frequencies obtained scaled by 0.9608 [36]. Gauss-View molecular visualization program was used to carry out vibrational band assignments [37].

To investigate the reactive sites of **III** the molecular electrostatic potentials were evaluated using B3LYP/6–31G(d,p) method. A preliminary search of low energy structures was carried out with B3LYP method using 6-31G(d,p) basis set. In addition, frontier molecular orbitals (FMO) for the title compound were performed with B3LYP/6-31G(d,p) the optimized structure.

3 Results and discussion

3.1 Description of the crystal structure

The crystal structure of **III** is monoclinic and space group P2₁/n, $M_w = 283.34$, a = 5.7387 Å, b = 23.842 Å, c = 10.3045 Å, $\beta = 104.655$, and V = 1364.0 Å³, Dx = 1.380 g/cm⁻³. Additional information for the structure determinations are given in **Table 3**. The molecule of (**III**) is non-planar. The triazole ring plane forms dihedral angles of 18.99 (7) and 89.35 (7)° with the hydroxyphenyl and benzyl substituent ring planes, respectively [C1–C6–C7–N2 = 17.1 (3)°, C5–C6–C7–N1 = 19.8 (3)°, C8–N1–C9–C10 = 98.6 (2)° and C7–N1–C9–C10 = –86.2 (3)°].

Table 3: Crystallographic data for title compound [16].

Chemical formula	C15H13N3OS
Formula weight	283.34
Temperature (K)	296
Crystal system	Monoclinic
Space group	P2 _{1/n}
Unit cell parameters	
a (Å)	5.7387(5)
b (Å)	23.842(3)
c (Å)	10.3045(9)
β(°)	104.655(6)
Volume (ų)	1364.0(2)
Z	4
Dcalc (g/cm³)	1.380
Crystal size (mm)	0.74 ×0.43×0.05
Reflections observed [I > $2\sigma(I)$]	1737
Data/parameters	2673/181
$R [F^2 > 2\sigma(F^2)]$	0.044
$wR(F^2)$	0.109
Goodness-of-fit on Indicator	0.87
Structure determination	SHELX97
Refinement	Full matrix
Δp max, Δp min (e/ Å ³)	0.16, -0.26

An intramolecular O–H···N hydrogen bond exists between the hydroxyphenyl group and the triazole N atom and N–H···S intermolecular hydrogen bonds are observed in the

crystal structure (**Table 4** and **Figure. 3**). An N3–H3···S1ⁱ hydrogen bond links inversion-related molecules into dimers. The N···S distance [3.287 (2) Å] in this interaction is shorter than the mean value of 3.44 (1) Å reported for such hydrogen bonds [38]. Also, the N–H···S angle (175°) is wider than the mean angle of 158 (1)°.

Table 4: Hydrogen bonding geometry (\mathring{A}, \circ) for the title compound.

D – H···A	D-H	H···A	D···A	D-H···A
N3 – H3···S1 ⁱ	0.86	2.43	3.287 (2)	175
O1 – H1···N2	0.82	1.91	2.631 (3)	146

Symmetry code: (i) 3 - x, -y, -z.

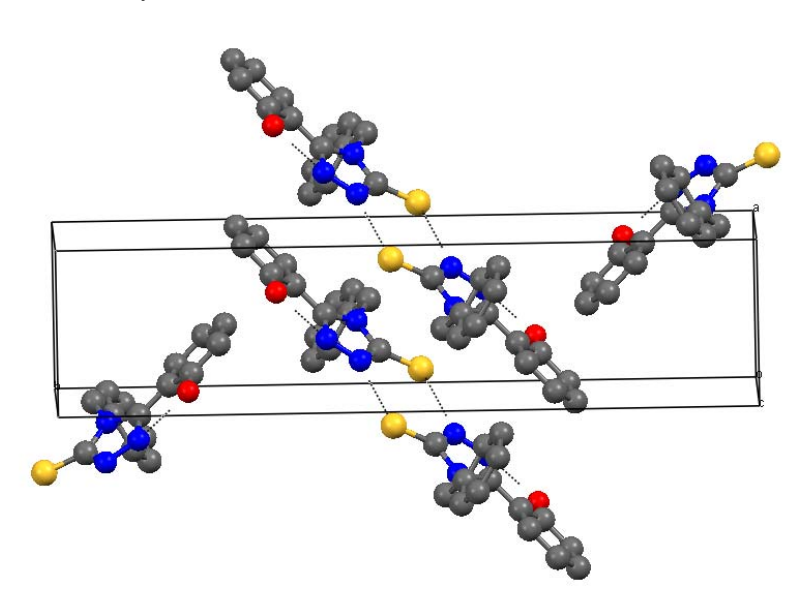


Figure 3: A packing diagram for title compound, showing the intermolecular interactions (dashed lines). Hydrogen atoms omitted for clarity.

3.2 Optimized geometry

The optimized parameters like bond lengths, bond angles, and dihedral angles of **III** were taken by using the B3LYP/6-31G(d,p) method. The atomic numbering design of the theoretical geometric structure is given in **Figure 4b**. The geometric parameters which accounted with the experimental data from the study are listed in **Table 5**. The slight conformational discrepancies are observed between the X-ray structure of **III** and its

optimized counterparts (see Figure 5). It is clear that the experimental results and the theoretical calculations are for the solid phase and for the gas phase sequentially. The existence of a crystal field along with the intermolecular interactions connects the molecules together, which results with some differences in bond parameters between the calculated and experimental values in solid state. The orientation of the phenyl ring of III proved the most notable discrepancy, and is defined with torsion angle N1-C9-C10-C11 [-14.2(3)°], which is calculated at -35.5° for B3LYP/6-31G(d,p) level.

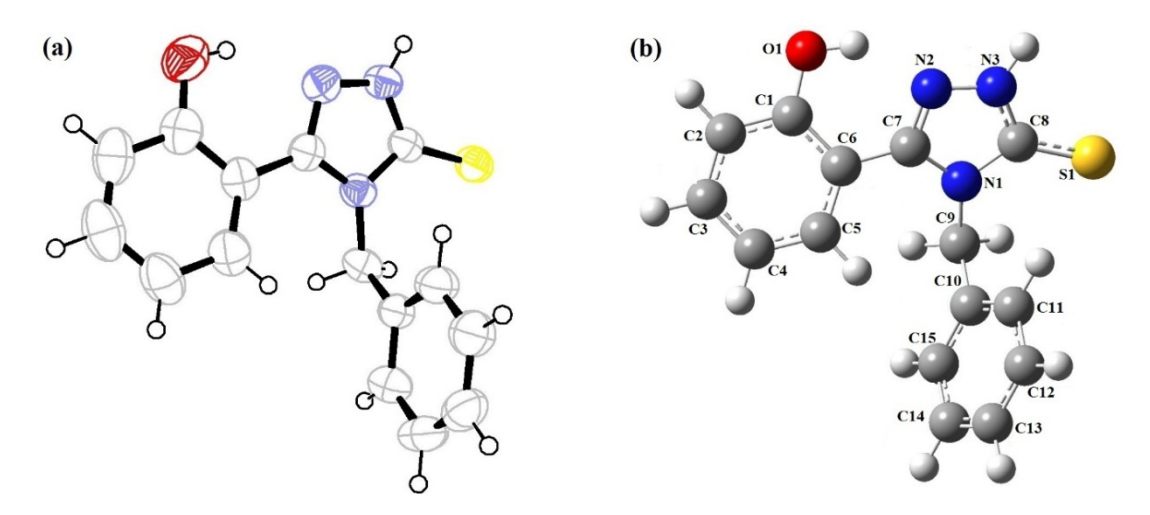


Figure 4: (a) Ortep-3 diagram of the title compound (b) The theoretical geometric structure of the title compound (with B3LYP/6–31G(d,p) level).

The structures obtained from theoretical calculations is globally compared through a logical method that superimposes molecular skeleton with what obtained from X-ray diffraction, which in conclusion gives a RMSE of 0.240 Å for B3LYP/6–31G(d,p) (Figure 5). This magnitude of RMSE can be explained by the fact that the intermolecular Coulombic interaction with the neighboring molecules are absent in gas phase, whereas the experimental result corresponds to interacting molecules in the crystal lattice [39].

Table 5: Selected molecular structure parameters.

Parameters	Experimental	B3LYP/6-31G(d,p)
Bond lengths (Å)		
S(1)-C(8)	1.673 (2)	1.671
O(1)-C(1)	1.355 (3)	1.348
N(1)-C(8)	1.379 (2)	1.395
N(1)-C(7)	1.385 (2)	1.392
N(1)-C(9)	1.461 (2)	1.467

N(2)-C(7)	1.308 (2)	1.317
N(2)-N(3)	1.368 (2)	1.364
N(3)-C(8)	1.334 (2)	1.355
C(6)-C(7)	1.458 (3)	1.465
C(9)-C(10)	1.500 (3)	1.518
RMSEa		0.001
Bond Angles (°)		
C(8)-N(1)-C(9)	121.40 (16)	121.62
C(7)-N(1)-C(9)	130.44 (16)	129.43
C(1)-C(6)-C(7)	119.48 (19)	118.90
C(5)-C(6)-C(7)	123.20 (20)	122.68
N(1)-C(9)-C(10)	114.47 (16)	115.55
RMSEa		0.516
Dihedral angles (°)		
C(1)-C(6)-C(7)-N(2)	17.1 (3)	22.1
C(5)-C(6)-C(7)-N(1)	19.8 (3)	25.9
C(8)-N(1)-C(9)-C(10)	98.6 (2)	99.0
C(7)-N(1)-C(9)-C(10)	-86.2(3)	-91.5

^a Between the bond lengths and the bond angles computed by the theoretical method and those obtained from X-ray diffraction.

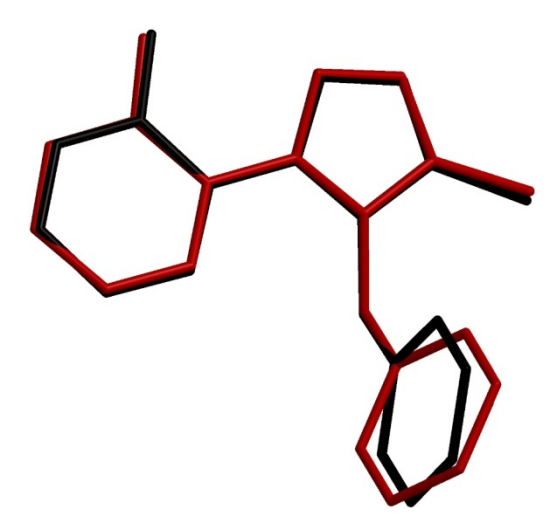


Figure 5: Atom-by-atom superimposition of the structures calculated (red) over the X-ray structure (black) for the title compound. Hydrogen atoms omitted for clarity.

3.3 IR spectroscopy

DFT/B3LYP method with 6–31G(d,p) basis set was used for calculating harmonic vibrational frequencies of **III**, and Gauss-View molecular visualization program for the vibrational band assignments. The vibrational frequencies were analyzed for facilitating the assignment of the observed peaks and the results of our calculation for **III** were compared with the experimental results (**Table 6**). The consistency of the experimental results with our calculations gives good conclusions in general.

Figure 6 shows its results. The OH group vibrations are found to be the possibly most sensitive to environment; therefore they show pronounced shifts in the spectra of the hydrogen-bonded species. The optimum absorption region of non-hydrogen-bonded or a free hydroxyl group is 3550–3700 cm⁻¹ regions [40]. In case of their presence in molecule, intra- and intermolecular hydrogen bonding reduces O–H stretching band to 3000–3550 cm⁻¹ region [41]. The IR spectra of **III** with an intense and relatively sharp band at maximum 3298 cm⁻¹ was assigned to the stretching vibrations of the sub-group in the intramolecular O H···N hydrogen bonds formed between N2 atom and O atom of hydroxyl group. This band has been calculated at 3368 cm⁻¹ for B3LYP level.

Table 6: Comparison of the experimental and calculated vibrational frequencies (cm-1).

Assignments	Experimental IR with KBr	B3LYP/6-31G(d,p)
v (N–H)	3216	3547
v (O–H)	3298	3368
v _s phenol (C–H)	3080	3110
v _s phenol (C–H)		3093
vs phenyl (C–H)		3091
v _{as} phenol (C–H)		3083
vas phenyl (C–H)		3071
v _{as} phenyl (C–H)		3061
vas phenyl (C–H)	3035	3049
$v_{as}(C-H)$	2995	3000
v _s (C–H)	2935	2938
v phenol (C=C)	1620	1610
v phenyl (C=C)		1598
v phenyl (C=C)		1578
v phenol (C=C)	1582	1570

v(C=N) + v(C=C)	1536	1522
γ (C–H) of phenyl	1490	1481
γ (C–H) of phenol		1478
γ (C–H) + α (C–H) + γ (N–H)		1453
γ (C–H) + ω (C–H) + γ (N–H)		1445
α (C-H)	1392	1421
ω (C–H)	1375	1370
δ (C–H) + v (N–N) + v (C–N)		1256
γ (C–H) of phenol + v (C–O)	1230	1250
v (C–N–C)	1150	1220
α phenyl (C–H)	1140	1166
α phenol (C–H)		1144
$v(N-N) + \alpha$ phenol (C–H)		1092
δ phenol (C–H)		962
v (C–C) of ethyl + δ (C–H)		941
δ (C–H)	740	823
δ (C–C-C) of phenol		726
δ (C–N-C) + δ (C–C-C)		703
δ (N-C-S)		657

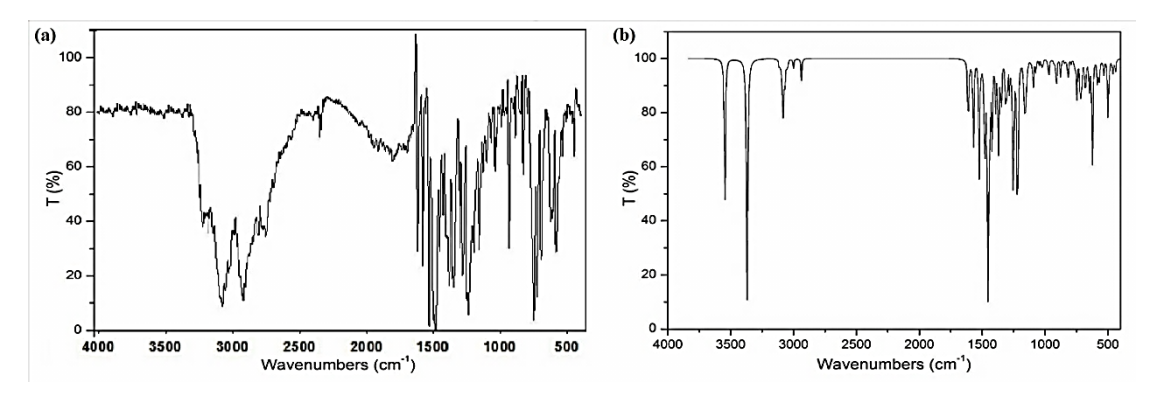


Figure 6: (a) FT-IR spectrum of the title compound. (b) Simulated B3LYP level IR spectra.

In the literature, some N–H stretching modes observed for the different substituent-triazole ring are 3383 cm⁻¹ [42] and 3417 cm⁻¹ [43] as experimentally. In our study, the N–H stretching mode was observed at 3216 cm⁻¹ which has a red shift and the cause of this shift is the intermolecular N3–H3···S1 hydrogen bonding. The red shifting is further enhanced by the reduction in the N–H bond order values, occurring due to donor–acceptor interaction [44]. These differences of O–H (70 cm⁻¹) and N–H stretching vibrations (331 cm⁻¹) occurred between the results of the experimental and calculations are due to the consideration of the isolated molecules (in gas phase) in the calculation method.

The aromatic C–H stretching, C–H in-plane bending and C–H out-of-plane bending vibrations appear in 2900–3150 cm⁻¹, 1100–1500 cm⁻¹ and 700–1000 cm⁻¹ frequency ranges, respectively. The C–H aromatic stretching mode was observed at 3080 cm⁻¹ experimentally, and calculated at 3110–3049 cm⁻¹ for B3LYP. The bands at 2995 cm⁻¹ correspond to the asymmetric stretching CH₂ modes. The C–H in-plane bending vibrations computed at 1481, 1370 and 1250 cm⁻¹ by B3LYP/6–31G(d,p) method shows excellent agreement with FT-IR bands at 1490, 1375 and 1230 cm⁻¹. The theoretically computed values of the angles bending vibration modes show good agreement with the experimental values. The other vibrational frequencies can be seen in **Table 6**.

3.4 NMR spectra

B3LYP method with 6–31G(d,p) basis set was used in order to calculate GIAO ¹H and ¹³C chemical shift values (with respect to TMS), which then compared with the experimental ¹H and ¹³C chemical shift values. **Table 7** shows the results of the aforementioned calculation.

Table 7: Theoretical and experimental 1H and 13C isotropic chemical shifts (with respect to TMS, all values in ppm) for the title compound.

Experimental (ppm) (DMSO-d ₆)	Calculated (ppm) B3LYP/6-31G(d,p)
153.21	151.88
110.87	111.78
123.30	125.54
109.10	111.15
124.56	121.94
102.14	104.8
145.04	145.99
166.43	167.89
45.27	49.82
131.36	130.54
120.87	121.07
122.05	122.55
124.75	120.89
120.05	121.51
117.29	119.79
5.16	4.74 and 6.41
6.79–7.34	7.13–8.11
	(DMSO-d ₆) 153.21 110.87 123.30 109.10 124.56 102.14 145.04 166.43 45.27 131.36 120.87 122.05 124.75 120.05 117.29 5.16

1H (<u>NH</u>)	13.94	9.13
1H (O- <u>H</u>)	10.40	10.32

We have calculated ¹H chemical shift values (with respect to TMS) of 10.32–4.74 ppm at B3LYP/6–31G(d,p) level, whereas the experimental results are observed to be 10.40–5.16 ppm. The singlet observed at 5.16 ppm is assigned to C(9)H₂ that has been calculated at 4.74 and 6.41 ppm. The aromatic protons resonate at 6.79–7.34 ppm multiplet experimentally, that have been calculated at 7.13–8.11 ppm. In different substituent-1,2,4-triazole, the H chemical shift of N–H were observed to be 11.33–13.56 ppm [45]. The NH hydrogen of the 1,2,4-triazole ring appears at 13.94 ppm, and is determined computationally at 9.13 ppm. The signal assigned to proton of the OH is observed at 10.40 ppm. This was calculated 10.32 ppm at B3LYP level. Because the intermolecular hydrogen bonds in molecular structure of III are neglected in the calculations, we can say that this difference between experimental and calculated chemical shifts is due to N–H···N intermolecular interactions.

We have calculated ¹³C chemical shift values (with respect to TMS) of 49.82–167.89 ppm with B3LYP/6-31G(d,p), while, the experimental results were observed to be 45.27–166.43 ppm. As can be seen from **Table 7**, theoretical ¹H and ¹³C chemical shift results of the title compound are generally closer to the experimental chemical shift data.

3.5 Molecular electrostatic potential

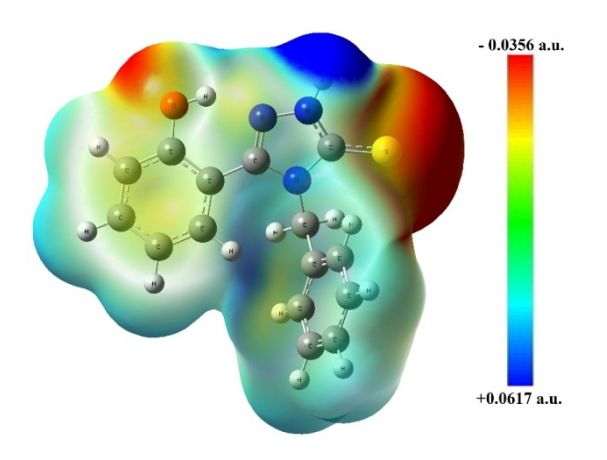
The formulation of molecular electrostatic potential (ESP) around a molecule at a point r in the space is (in atomic units)

$$V(r) = \sum_{A} \frac{Z_A}{|R_A - r|} - \int \frac{\rho(r)dr'}{|r'^{-r}|}$$

 Z_A is the charge on nucleus A located at R_A and $\rho(\mathbf{r})$ is the electron density. The first term in the expression represents the effect of the nuclei and the second represents that of electrons. The two terms have opposite signs and therefore opposite effects. V(r) is their resultant at each point r; it is an indication of the net electrostatic effect produced at the point r by the total charge distribution (electrons + nuclei) of the molecule. Electrostatic potential correlates with dipole moment, electronegativity, partial charges and site of chemical reactivity of the molecule. It provides a visual method to understand the relative polarity of a molecule. While the negative electrostatic potential corresponds to an attraction of the proton by the concentrated electron density in the molecule (and is colored in shades of red on the ESP surface), the positive electrostatic potential corresponds to repulsion of the proton by atomic nuclei in regions where low electron density exists and the nuclear charge is incompletely shielded (and is colored in shades of blue). By definition, electron density

isosurface is a surface on which molecule's electron density has a particular value and that encloses a specified fraction of the molecule's electron probability density. The electrostatic potential at different points on the electron density isosurface is shown by coloring the isosurface with contours. The graphical representation of the molecular electrostatic potential surface (MEP or ESP), as described by Politzer and Truhlar [46] is a series of values representing the evaluation of the interaction energy between a positively charged (proton) probe and points on a solvent accessible surface as defined by Connolly [47-49].

The electron density isosurface onto which the electrostatic potential surface has been mapped is shown in **Figure 7a** and **Figure 7b** for **III.** Such surfaces depict the size, shape, charge density and site of chemical reactivity of the molecules. The different values of the electrostatic potential at the surface are represented by different colors; red represents regions of most negative electrostatic potential, blue represents regions of most positive electrostatic potential and green represents regions of zero potential. Potential increases in the order red < orange < yellow < green < blue.



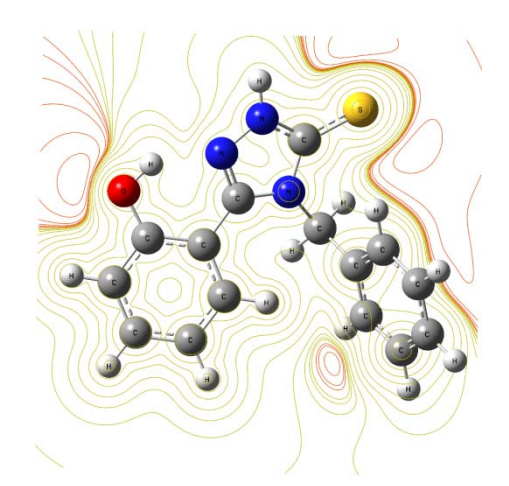


Figure 7a: Molecular electrostatic potential mapped on the ρ (r) = 0.0004 a.u. isodensity surface for **III**.

Figure7b: Molecular electrostatic potential mapped on the ρ (r) = 0.0004 a.u. isodensity surface for **III**.

Two projections of the ESP surfaces – one in molecular plane and the other in perpendicular planes – in the case of III are shown in **Figure 7a** and **Figure 7b**. Negative regions in the studied molecule were found around the O1 atom and S1 atom of triazole ring. The negative V(r) values are -0.035 a.u. for S1 atom, which is the most negative region, -0.033 a.u. for O1 atom which is a less negative region. However, a maximum positive region is localized on the H atom of the triazole ring with a value of +0.061 a.u. indicating a possible site for nucleophilic attack. According to these calculated results, the MEP map shows that the negative potential sites are on electronegative atoms as well as the positive potential sites are around the hydrogen atoms.

3.6 Frontier molecular orbitals

The energy of the LUMO is directly related to the electron affinity and characterizes the susceptibility of the molecule towards attack by nucleophiles [50]. An electron affinity (EA) refers to the capability of a legend to accept precisely one electron from a donor. However, to influence the interacting systems, covalent or hydrogen bonding may take place which can result in a partial charge transfer [51]. A current approximation is to use Koopman's theorem to express these quantities in terms of the frontier one electron energy levels: HOMO and LUMO [52–55]. The energy of the HOMO is directly related to the ionization potential (IP) and characterizes the susceptibility of the molecules towards attack by electrophiles. Hard nucleophiles have a low HOMO energy while hard electrophiles have a high LUMO energy [50]. The operational definition of LUMO and HOMO in the context of DFT can be written as:

 $EA = -\xi LUMO$

 $IP = -\xi HOMO$

where ξHOMO and ξLUMO correspond to the Kohn Sham [56] one electron eigen values associated to the frontier molecular orbital: HOMO and LUMO, respectively. IP and EA refer to ionization potential and electron affinity of the system respectively. The HOMO–LUMO energy values of **III** are shown in **Figure 8**. HOMO–LUMO energy gap is used as a quantum chemical descriptor in establishing correlations for chemical and biochemical systems [57]. A large HOMO–LUMO gap implies high stability for the molecules in the sense of its lower charge transfer in complexes. Polarizability is another characteristic property which is related to HOMO–LUMO energy gap. Soft molecules with small energy gap will be more polarizable than hard molecules. The comparatively lower value of the ELUMO-EHOMO (Fig. 8) of III shows that the molecule is polarizable and biologically active [58]. As seen from Fig. 8, both in the HOMO and HOMO–1, electrons are delocalized on the S1 atom and triazole ring. For the LUMO electrons are mainly delocalized on the triazole and phenol rings. The value of the energy separation between the HOMO and LUMO is -4.404 eV.

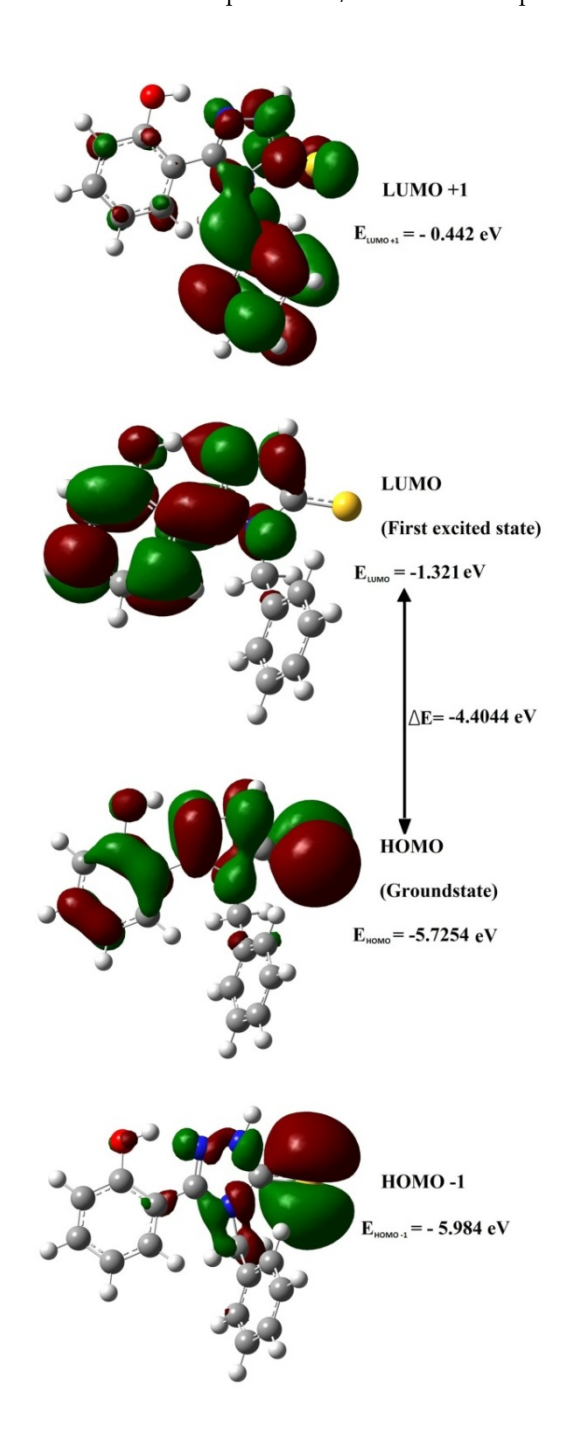


Figure 8: Molecular orbital surfaces and energy levels given in parentheses for the LUMO +1, LUMO, HOMO and HOMO -1 of the title compound computed at B3LYP/6-31G(d,p) level.

3.7 Conformational analysis

To define the preferential positions of phenol and phenyl ring with respect to triazole ring, a preliminary search of low energy structures was performed using DFT/B3LYP method with 6–31G(d,p) basis set as a function of the selected degrees of torsional freedom, ϕ_1 (NI-C9-C8-C11) and ϕ_2 (N2-C7-C6-C5). ϕ_1 and ϕ_2 dihedral angles are coordinates related to conformational flexibility. The respective values of the selected degrees torsional freedom, ϕ_1 (NI-C9-C8-C11) and ϕ_2 (N2-C7-C6-C5), are in optimized geometries -35.538 and -157.400°, respectively for B3LYP/6-31G(d,p). Energy maps with respect to rotations about (ϕ_1 , ϕ_2) torsion angles are presented in Figure 9a and 9b.

In these calculations, ϕ_1 and ϕ_2 were changed from -180° to +180° at a constant increment of 10°, and all other geometrical parameters were optimized. In consequence a flexible surface was obtained and shown in **Figure 9b**. **Figure 9b** indicates that there are four energy minima on the rotational potential energy surface of III.

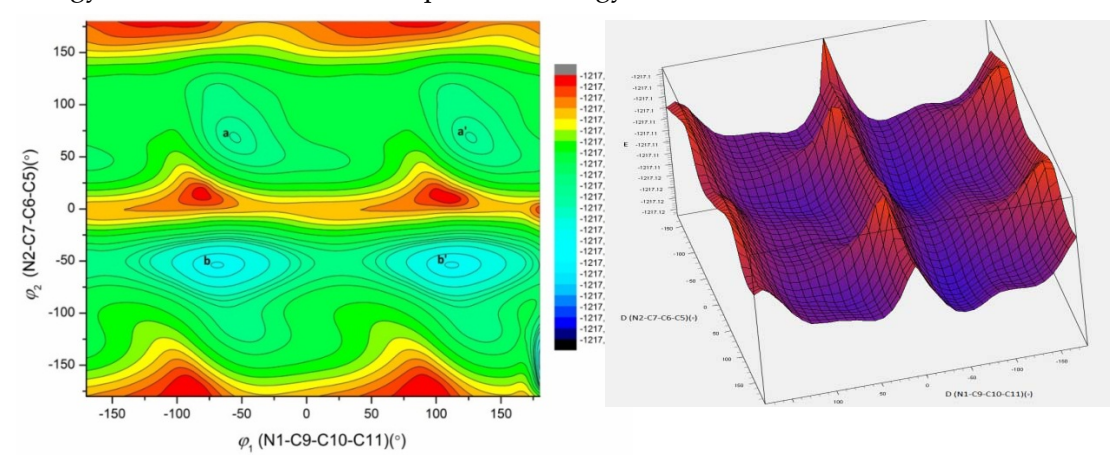


Figure 9a: Top view of the heat of formation surface for 4-benzyl-3-(2-hydroxyphenyl)-1H-1,2,4-triazole-5(4H)-thione

Figure 9b: The flexible potential energy surface of 4-benzyl-3-(2-hydroxyphenyl)-1H-1,2,4-triazole-5(4H)-thione

The parameters concerning minima have been given in **Table 8**. The low energy domains located around $\phi_1 = 0^\circ$ are symmetric images, so there are only two independent minima which are located at $\phi_1 = -55^\circ$, $\phi_2 = 68^\circ$ (a); $\phi_1 = -74^\circ$, $\phi_2 = -54^\circ$ (b). Energy difference between the most favorable and unfavorable conformers, which arises from rotational potential barrier calculated with respect to the selected torsion angle, was calculated as 0.0173 a.u.

Minimum	φ1 (NI-C9-C8-C11)	φ ₂ (N2-C7-C6-C5)	Total energy (a.u.)
a	-55	-68	-1217,11372
a'	127	68	-1217,11376
b	-70	-54	-1217,11621
b'	112	53	-1217,11623

Table 8: The minimums in the maps of the potential energy surfaces.

3.8 Biological study

3.8.1 Antibacterial and antifungal activity

The investigation of antibacterial and antifungal screening data revealed that the title compound showed good inhibition at 1.56–25 mg/mL in DMSO. The screening result indicates that title compound tested exhibited significant antibacterial and antifungal activities when compared with the reference drug. The title compound was found to be same potent as the reference drug, ciprofloxacin, in case of *P. aeruginosa*.

Structure and biological activity relationship of title compound showed that presence of hydroxy groups attached to phenyl ring to the triazole ring of the title compound is responsible for good antimicrobial activity [59]. In conclusion the present study showed that the synthesized compound can be used as template for future development through modification and derivatization to design more potent and selective antimicrobial agents.

3.8.2 Antioxidant activity

It has been reported that the antioxidant activity of the phenolic compounds depends on their molecular structure, especially on their hydrogen-donating ability and subsequent stabilization of the formed phenoxy radical [60]. As shown in **Table 9**, the title compound has scavenging activity between 45.5% and 85.3% within the investigated concentration range. The antioxidant activity of the title compound is obvious that the scavenging activity increases with increasing sample concentration in the range tested. This activity can be explained on the basis of their structure as these derivatives posses phenolic hydroxyls which are available as hydrogen donors to the DPPH radical.

Table 9: Antioxidant scavenging activity data of the title compound on DPPH ● free radical at different concentrations.

T. 1. 1. C	DPPH scavenging activity (%)				
Tested Compound	62.5 μΜ	125 μΜ	187.5 μΜ	250 μΜ	312.5 μM
Title Compound	45.5 ± 0.2	57.4 ± 0.3	70.9 ± 0.3	78.2 ± 0.1	85.3 ± 0.1
Ascorbic acid ^a	55.0 ± 0.2	65.0 ± 0.2	75.0 ± 0.2	85.0 ± 0.2	95.0 ± 0.2

^a Ascorbic acid, was used as a standard.

4 Conclusions

The investigation of the present work is illuminate the spectroscopic properties such as molecular parameters, frequency assignments and magnetic properties of title compound by using FT-IR, ¹H and ¹³C NMR techniques and tools derived from the density functional theory. The synthesis and analysis of such substances both experimental and theoretically has been important contribution in field of computational materials science and technology. Due to the lack of experimental information on the structural parameters available in the literature, the optimized geometric parameters (bond lengths and bond angles) was theoretically determined at B3LYP/6-31G(d,p) level of theory and compared with the structurally similar compounds. The X-ray structure is found to be very slightly different from its optimized counterpart, and the crystal structure is stabilized by N-H···S and O-H···N hydrogen bonds. It was noted here that the experimental results belong to solid phase and theoretical calculations belong to gaseous phase. In the solid state, the existence of the crystal field along with the intermolecular interactions have connected the molecules together, which result in the differences of bond parameters between the calculated and experimental values. Despite the differences observed in the geometric parameters, the general agreement is good and the theoretical calculations support the solid-state structure. The vibrational FT-IR spectrum of the III was recorded and computed vibrational wavenumbers. The magnetic properties of the title molecule were observed and calculated the same method. The chemical shifts were compared with experimental data in DMSO solution, showing a very good agreement both for ¹³C and ¹H chemical shifts. When all theoretical results scanned, they are showing good correlation with experimental data. The antimicrobial activity study revealed that the title compound showed good antibacterial and antifungal activities against pathogenic strains. The antioxidant activity of the title compound is obvious that the scavenging activity increases with increasing sample concentration in the range tested.

References

- [1]S. Calitano, F. Piacenti, G. Sbrana, The vibrational spectrum of isothiazole, Spectrochim. Acta, 20 (1964), 339-344.
- [2]F. Billes, H. Endredi, G. Jalsocesyky, Vibrational spectroscopy of diazoles, J. Mol Struc-Theochem, 465 (1999), 157-172.
- [3]J. Sandstrom, Recent advances in the chemistry of 1,3,4-thiadiazoles, Adv. Heterocycl. Chem., 9 (1968), 165-209.
- [4]M. Koparir, A. Cansiz, A. Cetin, Synthesis and spectral investigations of 2,5,7-triaryl-5H-[1,3,4]thiadiazolo[3,2-alpha]pyrimidin-6[7H]-ones, Asian J Chem, 17 (2005), 1689-1697.
- [5] Cansiz, S. Servi, M. Koparir, M. Altintas, M. Digrak, Synthesis and biological activities of some mannich bases of 5-(2-furyl)-1,2,4-triazole-3-thiones, J. Chem. Soc. Pakistan., 23 (2001), 237-240.
- [6]M. D. Mullicon, M. W. Wilson, D. T. Connor, C. R. Kostlan, D. J. Schrier, R. D. Dyer, Design of 5-(3,5-di-tert-butyl-4-hydroxyphenyl)-1,3,4-thiadiazoles, 5-(3,5-di-tert-butyl-4-hydroxyphenyl)-1,2,4-triazoles as orally-active, nonulcerogenic antiinflammatory agents, J. Med. Chem., 36 (1993), 1090-1099.
- [7]R. D. Porsolt, A. Bertin, M. Jalfre, Behavioral despair in mice: a primary screening test for antidepressants., Arch. Int. Pharmacol., 229 (1977), 327-336.
- [8]S. A. Shans El-Dine And A. A. B. Hazzaa, Synthesis of compounds with potential fungicidal activity .2, Pharmazie, 29 (1974), 761-763.
- [9]J. K. Sugden, T. Yoloye, Medicinal applications of indole-derivatives, Pharm. Acta Helv., 53 (1978), 65-92
- [10] P. C. Unangst, G. P. Shurum, D. T. Connor, R. D. Dyer, D. J. Schrier, Novel 1,2,4-oxadiazoles and 1,2,4-thiadiazoles as dual 5-lipoxygenase and cyclooxygenase inhibitors, J. Med. Chem., 35 (1992), 3691-3698.
- [11] S. Genc, N. Dege, A. Cetin, A. Cansiz, M. Sekerci And M. Dincer, 3-(2-Hydroxypheny1)-4-pheny1-1H-1,2,4-triazole-5(4H)-thione, Acta Cryst., E60 (2004), o1580-o1582.
- [12] W. Li, Q. Wu, Y. Ye, M. Luo, L. Hu, Y. Gu, F. Niu And J. Hu, Density functional theory and ab initio studies of geometry, electronic structure and vibrational spectra of novel benzothiazole and benzotriazole herbicides, Spectrochim. Acta A., 60 (2004), 2343-2354.
- [13] B. Mernari, H. Elattari, M. Triasnel, F. Bentiss And M. Langrenee, Inhibiting effects of 3,5-bis(n-pyridyl)-4-amino-1,2,4-triazoles on the corrosion for mild steel in 1M HCl medium, Corros. Sci., 40 (1998), 391-399.
- [14] F. Bentiss, M. Langrenes, M. Traisnel, J. C. Hornez, The corrosion inhibition of mild steel in acidic media by a new triazole derivative, Corros. Sci., 41 (1999), 789-803.

- [15] S. Ozturk, M. Akkurt, A. Cansiz, M. Koparir, M. Sekerci, F. W. Heinemann, 3-Benzyl-4-(4-chlorophenyl)-1H-1,2,4-triazole-5(4H)-thione, Acta Cryst E60 (2004), o642-o644.
- [16] N. Dege, A. Cetin, A. Cansiz, M. Sekerci, C. Kazaz, M. Dincer, O. Buyukgungor, 4-Benzyl-3-(2-hydroxyphenyl)-1H-1,2,4-triazole-5(4H)-thione, Acta Cryst. E60 (2004), o1883-o1885
- [17] M. H. Klingele, S. Brooker, The coordination chemistry of 4-substituted 3,5-di(2-pyridyl)-4H-1,2,4-triazoles and related ligands, Coord. Chem. Rev., 241 (2003), 119-132.
- [18] U. Beckmann, S. Brooker, Cobalt(II) complexes of pyridazine or triazole containing ligands: spin-state control, Coord. Chem. Rev., 245 (2003), 17-29.
- [19] R. N. Muller, L. V. Elst, S. Laurent, Spin transition molecular materials: Intelligent contrast agents for magnetic resonance imaging, J. Am. Chem. Soc., 125 (2003), 8405-8407.
- [20] S. Komeda, S. Bombard, S. Perrier, J. Reedijk, J. Kozelka, Kinetic study of azole-bridged dinuclear platinum(II) complexes reacting with a hairpin-stabilized double-stranded oligonucleotide, J. Inorg. Biochem., 96 (2003), 357-366.
- [21] F. D. Proft, P. Geerlings, Conceptual and computational DFT in the study of aromaticity, Chem. Rev., 101 (2001), 1451–1464.
- [22] C. Orek, P. Koparir, M. Koparir, N-cyclohexyl-2-[5-(4-pyridyl)-4-(p-tolyl)-4h-1,2,4-triazol-3-ylsulfanyl]-acetamide dihydrate: synthesis, experimental, theoretical characterization and biological activities, Spectrochim. Acta A., 97 (2012), 923–934.
- [23] Cansiz, A. Cetin, C. Orek, M. Karatepe, K. Sarac, A. Kus, P. Koparir, 6-Phenyl-3-(4-pyridyl)-1,2,4-triazolo-[3,4-b][1,3,4]thiadiazole: synthesis, experimental, theoretical characterization and biological activities, Spectrochim. Acta A., 97 (2012), 607–615.
- [24] H. Tanak, DFT computational modeling studies on 4-(2,3-dihydroxybenzylideneamino)-3-methyl-1h-1,2,4-triazol-5(4h)-one, Comput. Theor. Chem., 967 (2011), 93–101.
- [25] G. Fitzgerald And J. Andzelm, Chemical applications of density functional theory comparison to experiment, hartree-fock, and perturbation-theory, J. Phys. Chem., 95 (1991), 10531–10534.
- [26] J. Andzelm, E. Wimmer, Density functional gaussian-type-orbital approach to molecular geometries, vibrations, and reaction energies, J. Chem. Phys., 96 (1992), 1280–1303.
- [27] Barry, Procedures and theoretical considerations for testing antimicrobial agents in agar media, in: Lorian (Ed.), Antibiotics in Laboratory Medicine, fifth ed. Williams and Wilkins, Baltimore, 1991 (MD, 1).
- [28] D. J. Maclowry, M. J. Jaqua And S. T. Selepak, Detailed methodology and implementation of a semiautomated serial dilution microtechnique for antimicrobial susceptibility testing, Appl. Microbiol., 20 (1970), 46-53.
- [29] C. H. Fenlon, M. H. Cynamon, Comparative invitro activities of ciprofloxacin and other 4-quinolones against mycobacterium-tuberculosis and mycobacterium-intracellulare, Antimicrob. Agents Chemother., 29 (1986), 386-388.

- [30] R. Davis, A. Markam, J. A. Balfour, Ciprofloxacin An updated review of its pharmacology, therapeutic efficacy and tolerability, Drugs, 51 (1996), 1019-1074.
- [31] B. A. Arthington-Skaggs, M. Motley, D. W. Warnock, C. J. Morrison, Comparative evaluation of pasco and national committee for clinical laboratory standards m27-a broth microdilution methods for antifungal drug susceptibility testing of yeasts, J. Clin. Microbiol., 6 (2000), 2254-2260.
- [32] M. M. Hossain, M. F. Aziz, R. Ahmed, M. Hossain, A. Mahmuda, T. Ahmed, M. H. Mazumder, In vitro free radical scavenging activity of some β -lactams and phenolics, Int. J. Pharm., Sci., 2 (2010), 60–63.
- [33] M. J. Frisch, G. W. Trucks, H. B. Schlegel, G. E. Scuseria, M. A. Robb, J. R. Cheeseman, G. Scalmani, V. Barone, B. Mennucci, G.A. Petersson, H. Nakatsuji, M. Caricato, X. Li, H. P. Hratchian, A. F. Izmaylov, J. Bloino, G. Zheng, J. L. Sonnenberg, M. Hada, M. Ehara, K. Toyota, R. Fukuda, J. Hasegawa, M. Ishida, T. Nakajima, Y. Honda, O. Kitao, H. Nakai, T. Vreven, J. A. Montgomery, Jr., J. E. Peralta, F. Ogliaro, M. Bearpark, J.J. Heyd, E. Brothers, K. N. Kudin, V. N. Staroverov, R. Kobayashi, J. Normand, K. Raghavachari, A. Rendell, J. C. Burant, S. S. Iyengar, J. Tomasi, M. Cossi, N. Rega, J. M. Millam, M. Klene, J. E. Knox, J. B. Cross, V. Bakken, C. Adamo, J. Jaramillo, R. Gomperts, R. E. Stratmann, O. Yazyev, A. J. Austin, R. Cammi, C. Pomelli, J. W. Ochterski, R. L. Martin, K. Morokuma, V. G. Zakrzewski, G. A. Voth, P. Salvador, J. J. Dannenberg, S. Dapprich, A. D. Daniels, O. Farkas, J. B. Foresman, J. V. Ortiz, J. Cioslowski, D. J. Fox, Gaussian, Inc., Wallingford CT, 2009.
- [34] H. B. Schlegel, Optimization of equilibrium geometries and transition structures, J. Comput. Chem., 3 (1982), 214–218.
- [35] C. Peng, P. Y. Ayala, H. B. Schlegel, M. J. Frisch, Using redundant internal coordinates to optimize equilibrium geometries and transition states, J. Comput. Chem., 17 (1996), 49–56.
- [36] NIST Chemistry Webbook, IR database, http://srdata.nist.gov/cccbdb.
- [37] R. Dennington, T. Keith, J. Millam, GaussView, Version 4.1.2, Semichem, Inc., Shawnee Mission, KS, 2007.
- [38] F. H. Allen, C. M. Bird, R. S. Rowland, P. R. Raithby Resonance-induced hydrogen bonding at sulfur acceptors in R1R2C=C and R1CS2- systems, Acta Cryst., B53, (1997), 680-695.
- [39] H. Tanak, Crystal structure, spectroscopy, and quantum chemical studies of (e)-2[(2-chlorophenyl)iminomethyl]-4-trifluoromethoxyphenol, J. Phys. Chem., A115 (2011), 13865–13876.
- [40] C. Y. Panicker, H. T. Varghese, K. R. Ambujakshan, S. Mathew, S. Ganguli, A. K. Nanda, C. Van Alsenoy, FT-IR and FT-Raman spectra and ab initio calculations of 3-{[(2-hydroxyphenyl)methylene]amino}-2-phenylquinazolin-4(3H)-one, J. Raman Spectrosc., 40 (2009), 1262-1273.
- [41] Teimouri, A. N. Chermahini, K. Taban, H. A. Dabbagh, Experimental and CIS, TD-DFT, ab initio calculations of visible spectra and the vibrational frequencies of sulfonyl azide-azoic dyes, Spectrochim. Acta A., 72 (2009), 369–377.

- [42] R. Ustabas, N. Suleymanoglu, H. Tanak, Y.B. Alpaslan, Y. Unver And K. Sancak, Experimental and theoretical studies of the molecular structure of 4-(3-(1H-imidazol-1-yl)propyl)-5-p-tolyl-2H-1,2,4-triazol-3(4H)-one, J. Mol. Struct., 984 (2010), 137–145.
- [43] K. Sancak, Y. Unver, H. Tanak, İ. Degirmencioglu, E. Dugdu, M. Er, S. Isik, The synthesis of some new imidazole and triazole derivatives: crystal Structure and DFT-TDDFT investigation on electronic structure, J. Inclusion Phenom. Macrocycl. Chem., 67 (2010), 325–334.
- [44] Y. Koysal, H. Tanak, Crystal structure, spectroscopic investigations and density functional studies of 4-(4-methoxyphenethyl)-5-benzyl-2H-1,2,4-triazol-3(4H)-one monohydrate, Spectrochim. Acta A., 93 (2012), 106–115.
- [45] P. J. Garratt, In: A. R. Katritzky, C. W. Rees, E. F. V. Scriven (Eds.), Comprehensive Heterocyclic Chemistry II, vol. 4, Elsevier Science Ltd, 1996, pp. 127–163.
- [46] P. Politzer, D. G. Truhlar (Eds.), Chemical applications of atomic and molecular electrostatic potentials, Plenum Press, New York, 1981.
- [47] B. Chattopadhyay, S. Basu, P. Chakraborty, S. K. Choudhuri, A. K. Mukherjee, M. Mukherjee, Synthesis, spectroscopic characterization, X-ray powder structure analysis, DFT study and in vitro anticancer activity of N-(2-methoxyphenyl)-3-methoxysalicylaldimine, J. Mol. Struc. 932 (2009), 90-96.
- [48] U. C. Singh, P. A. Kollman, An approach to computing electrostatic charges for molecules, J. Comput. Chem. 5 (1984), 129-145.
- [49] M. L. Connolly, Solvent-accessible surfaces of proteins and nucleic-acids, Science 221 (1983), 709-713.
- [50] M. Karelson, V.S. Lobanov, Quantum-chemical descriptors in QSAR/QSPR studies, Chem. Rev., 96 (1996), 1027-1043.
- [51] P. Thanikaivelan, V. Subramanian, V. R. Raghava, B. N. Unni, Application of quantum chemical descriptor in quantitative structure activity and structure property relationship, Chem. Phys. Lett. 323 (2000), 59-70.
- [52] R. Contreras, P. Fuentealba, M. Galvan And P. Perez, A direct evaluation of regional Fukui functions in molecules, Chem. Phys. Lett. 304 (1999), 405-413.
- [53] P. Fuentealba, R. Contreras, Reviews of modern quantum chemistry, in: K.D. Sen (Ed.), World Scientific, Singapore, 2002 (vol. II).
- [54] P. Fuentealba, P. Perez, R. Contreras, On the condensed Fukui function, J. Chem. Phys., 113 (2000), 2544-2551.
- [55] Fleming, Frontier orbitals and organic chemical reactions, John Wiley and Sons, New York, 1976.
- [56] W. Kohn, L. Sham, Self-consistent equations including exchange and correlation effects, J. Phys. Rev. 140 (1965), A1133- A1138.
- [57] N. Z. Francisco, V. R. Ricardo, Ab initio study of luminescent substituted 8-hydroxyquinoline metal complexes with application in organic light emitting diodes J. Mol. Struct-Theochem. 850 (2008), 127-134.

- [58] L. Padmaja, C. Ravikumar, D. Sajan, I. Hubert Joe, V. S. Jayakumar, G. R. Pettit And O. Faurskov, Density functional study on the structural conformations and intramolecular charge transfer from the vibrational spectra of the anticancer drug combretastatin-A2, Nielsen, J. Raman Spectrosc., 40 (2009), 419-428.
- [59] Q. Ding, L. Zhang, H. Zhang, Synthesis and biological activities of some novel triazolothiadiazines and schiff bases derived from 4-amino-3-(4-hydroxyphenyl)-1h-1,2,4-triazole-5(4h)-thione, Phosphorus Sulfur, 185 (2010), 567–572.
- [60] F. Borges, F. A. M. Silva, C. Guimaraes, J. L. F. C. Lima, C. Matos, S. Reis, Phenolic acids and derivatives: studies on the relationship among structure, radical scavenging activity, and physicochemical parameters, J. Agric. Food Chem., 48 (2000), 2122-2126.